




Article

Double Electromagnetically Induced Transparency and Its Slow Light Application Based on a Guided-Mode Resonance Grating Cascade Structure

Guofeng Li ^{1,2}, Junbo Yang ², Zhaojian Zhang ², Yuyu Tao ¹, Lingjun Zhou ¹, Huimin Huang ¹, Zhenrong Zhang ^{1,*} and Yunxin Han ^{2,*}

¹ Guangxi Key Laboratory of Multimedia Communications and Network Technology, School of Computer, Electronics and Information, Guangxi University, Nanning 530004, China; 1813391006@st.gxu.edu.cn (G.L.); taoyuyu@st.gxu.edu.cn (Y.T.); 1813391017@st.gxu.edu.cn (L.Z.); 1813301006@st.gxu.edu.cn (H.H.)

² Center of Material Science, National University of Defense Technology, Changsha 410073, China; yangjunbo@nudt.edu.cn (J.Y.); 376824388@alumni.sjtu.edu.cn (Z.Z.)

* Correspondence: zrz76@gxu.edu.cn (Z.Z.); hanyx15@nudt.edu.cn (Y.H.); Tel.: +86-159-7816-9432 (Z.Z.); +86-137-5509-0901 (Y.H.)

Received: 15 July 2020; Accepted: 18 August 2020; Published: 21 August 2020



Abstract: In recent years, the achievement of the electromagnetically induced transparency (EIT) effect based on the guided-mode resonance (GMR) effect has attracted extensive attention. However, few works have achieved a double EIT-like effect using this method. In this paper, we numerically achieve a double EIT-like effect in a GMR system with a three-layer silicon nitride waveguide grating structure (WGS), using the multi-level atomic system model for theoretical explanation. In terms of slow light performance, the corresponding two delay times reach 22.59 ps and 8.43 ps, respectively. We also investigate the influence of wavelength detuning of different GMR modes on the transparent window and slow light performance. Furthermore, a wide-band flat-top transparent window was also achieved by appropriately adjusting the wavelength detuning between GMR modes. These results indicate that the EIT-like effect in the WGS has potential application prospects in low-loss slow optical devices, optical sensing, and optical communications.

Keywords: guided-mode resonance; electromagnetically induced transparency; waveguide grating structure; slow light

1. Introduction

The electromagnetically induced transparency (EIT) effect is caused by quantum interference of different excitation paths in a three-level system; it is also one of the important technologies to achieve the slow light effect [1,2]. The EIT effect happens where the pump light passes through the medium without absorption under the action of strong resonance coupling light. Similar to EIT is extraordinary light transmission (ELT), which can add an external magnetic field to make light pass through the opaque film with high transmission [3]. The transparent window of EIT is usually accompanied by extremely strong dispersion [4].

Over the past few decades, the EIT effect has aroused the interest of many researchers due to its unique ability to reduce and control the speed of light [5–7]. In addition, EIT has many potential applications in sensing [7], nonlinear optics [8], and cavity quantum electrodynamics [9]. Researchers have to resort to classic optical systems for an EIT-like effect, since EIT effects in atomic energy systems happen under strict experimental conditions, such as ultra-low temperature, hence limiting their practical application. Shanhui Fan successfully accomplished the EIT-like effect in an optical microcavity system in 2002 [10], and there has been increasing work using this approach to implement the EIT-like

effect [11,12]. Since then, EIT-like effects have also been achieved in plasmonic systems [13,14] and metamaterial structures [15,16]. Sun-Goo Lee developed the EIT-like effect based on the guided-mode resonance (GMR) effect in a waveguide grating structure (WGS), which contains two planar dielectric waveguides and a sub-wavelength grating [17], where the transparent window appears in the transmission dip by coupling high-Q and low-Q resonance modes in different dielectric waveguides.

In recent years, there has been much research interest in obtaining EIT-like effects by utilizing the GMR effect. Sun-Goo Lee presented two photonic systems that make it possible to achieve the GMR-based polarization-independent EIT-like effect, with both systems including two planar dielectric waveguides and a two-dimensional photonic crystal [18]. Yaru Sun reported a new planar metamaterial composed of a two-ring-resonator unit cell based on the GMR effect to achieve an EIT-like effect [19]. Han achieved an EIT-like effect with a Q value of 288,892 in a GMR system that includes two silicon grating waveguide layers stacked on CaF₂ substrates [20]. Previously, we reported a double EIT-like effect with two high Q values in a GMR system, where both waveguide layers have two dielectric gratings in one period, and two narrow-band transparent windows appear in the two transmission dips on account of the coupling of different GMR modes [21]. However, few works have achieved a double EIT-like effect by taking advantage of the GMR effect in a WGS. In recent years, cascade resonant grating has attracted extensive attention and research due to its versatility. Not only can it be used to design filters [22–24], but optical phenomena very similar to EIT characteristic spectra were also observed in some work [24–26]. Therefore, it will be an interesting topic to study the EIT-like effect combining the characteristics of the GMR effect and cascade resonant grating.

In this paper, a double EIT-like effect is investigated numerically based on a GMR system including three silicon nitride (Si₃N₄) grating waveguide layers (GWLs) stacked on SiO₂ substrates. Compared with our previous research [21], this work makes two transparent windows appear simultaneously in a transmission dip. The corresponding optical phenomenon can be explained by the multi-level atomic energy system model. We have discussed the dual-channel slow light performance of the system. We also present the effect of wavelength detuning of different GMR modes on the position of the transparent window and slow light performance by changing the grating width. Moreover, a broadband flat-top transparent window can be obtained through an appropriate detuning of the response wavelength between GMR modes. This work paves the way for high-performance slow light devices and has potential applications in optical communications.

2. Materials and Methods

The optical characteristics of the GMR system were investigated by the three-dimensional (3D) finite-difference time-domain (FDTD) method. The mesh accuracy was set to $\lambda/26$ to maintain the convergence of all simulation results. The schematic diagram of the GMR system with triple cascaded resonant gratings is shown in Figure 1a. The “Boundary conditions” were “Periodic” in the X and Y directions, and “perfectly matched layer (PML)” in the Z direction. The mesh accuracy in the three GWLs were $\Delta x = 10$ nm and $\Delta z = 20$ nm. The refractive index data of SiO₂ [27] and Si₃N₄ [28] were derived from the original publication. The background refractive index of the system was $n_s = 1$.

The light entered the system vertically and was a plane wave polarized in the X direction (TM polarization) in the near-infrared band. The period P of the grating was 809 nm. The thickness t of the Si₃N₄ waveguide was set to 900 nm. The three gratings (G_1, G_2, G_3) had a depth D of 200 nm and a width of 400 nm (i.e., $W_1 = W_2 = W_3$). In other words, the parameters of the three GWLs were exactly consistent. A SiO₂ layer with a thickness d_1 of 630 nm was placed on the top layer of the structure in order to reduce the reflected light. The distance d_2 between GWL₁ and GWL₂ was 690 nm; the distance d_3 between GWL₂ and GWL₃ was also 690 nm.

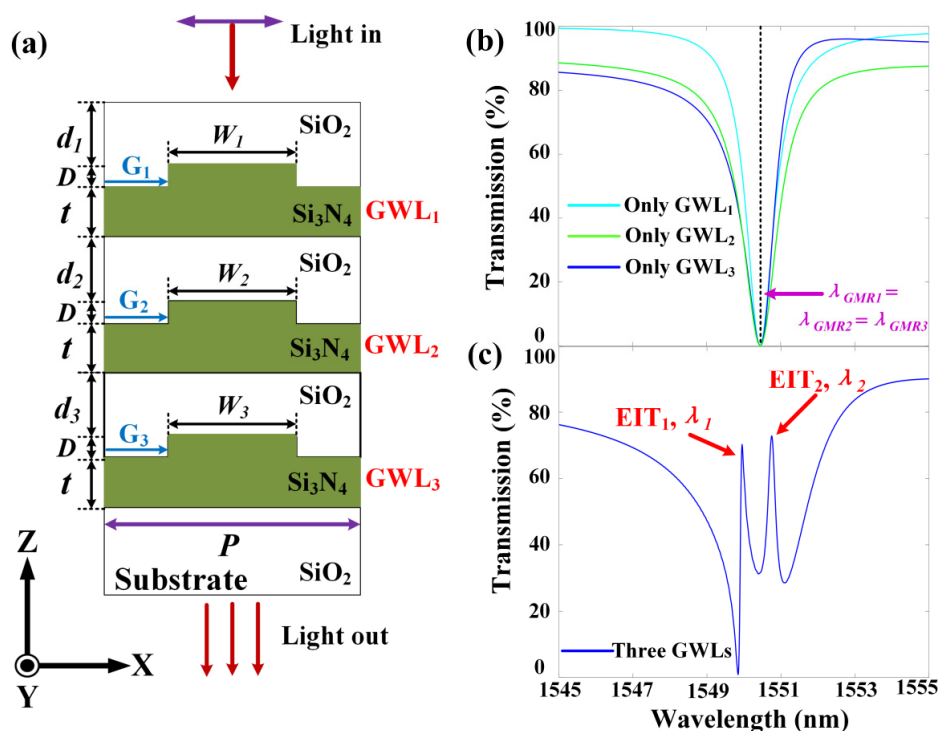


Figure 1. (a) Schematic diagram of the guided-mode resonance (GMR) system with three grating waveguide layers (GWLs); the geometric parameters are $d_1 = 630$ nm, $d_2 = 690$ nm, $d_3 = 690$ nm, $D = 200$ nm, $t = 900$ nm, $W_1 = W_2 = W_3 = 400$ nm, period $P = 809$ nm; (b) Transmission spectra of only GWL₁ or only GWL₂ or only GWL₃; (c) Transmission spectrum when all three GWLs are present.

3. Results

We firstly calculated the transmission spectrum when there was only a single GWL in the GMR system. The corresponding transmission spectra are shown in Figure 1b. The solid lines of cyan, blue, and green are the transmission spectra of GWL₁, GWL₂, and GWL₃, respectively. They all had a transmission dip with a center wavelength of 1550.44 nm ($\lambda_{GMR1} = \lambda_{GMR2} = \lambda_{GMR3}$), which exhibits GMR characteristics of wide resonance and high reflection. However, their sideband transmittances were slightly different because their optical properties are easily affected by the surrounding medium. The top SiO₂ layer had an effect on the resonance wavelengths of guide modes. To this end, the thickness of the SiO₂ coating layer was adjusted to the appropriate parameters not only to ensure that the three GWLs had the same resonance wavelength, but also to maximize the transmittance of incident light [20].

When all three GWLs are present and the top GMR mode (in GWL₁) couples with two other GMR modes (the middle GMR mode in GWL₂ and the bottom GMR mode in GWL₃), two sharp EIT-like characteristic resonances will appear simultaneously in the transmission dip that is caused by guided-mode resonance. The optical phenomenon resulting from the coupling of different GMR modes is the EIT-like spectral response, where two narrow transparent windows appear simultaneously in the stop band due to destructive interference [14,20,29]. The two EITs (denoted as EIT₁ and EIT₂ in Figure 1c) had respective resonance wavelengths λ_1 and λ_2 of 1549.95 nm and 1550.75 nm, and their transmittances reached 70.24% and 72.84%. The full widths at half maximum (FWHM) of the two EITs were 0.17 nm and 0.20 nm, respectively. Therefore, the Q factors of the two EITs were 9117 and 7753, respectively. Compared with the previous work that accidentally observed EIT-like characteristic spectra in several resonant grating structures [24,25], it is clear that we successfully used the GMR effect to achieve a double EIT-like effect with a narrow band and a high Q value in the resonance grating cascade structure.

In order to explore the mechanism of the observed double EIT-like effect, the electric field distribution of the double EIT peaks is shown in Figure 2a. It can be distinctly noticed that for the the EIT₁ electric field, extremely strong coherent resonance appears in both GWL₁ and GWL₂, while for EIT₂, strong coherent resonance mainly occurs in GWL₁ and GWL₃. At the resonance wavelength of EIT₁ (EIT₂), light is reflected back and forth between GWL₁ and GWL₂ (GWL₃), and electromagnetic energy is coupled into GWLs with strong coherent resonance excited by modes coupling. The top GMR mode is coupled with the other two modes when Fabry–Pérot (F–P) resonance is introduced once the optical distance between grating G₁ and grating G₂ (G₃) satisfies the phase matching condition [20,25,30], as shown in the following equation:

$$\varphi = \frac{2\pi \cdot n_{eff} \cdot S}{\lambda} = m\pi \quad (1)$$

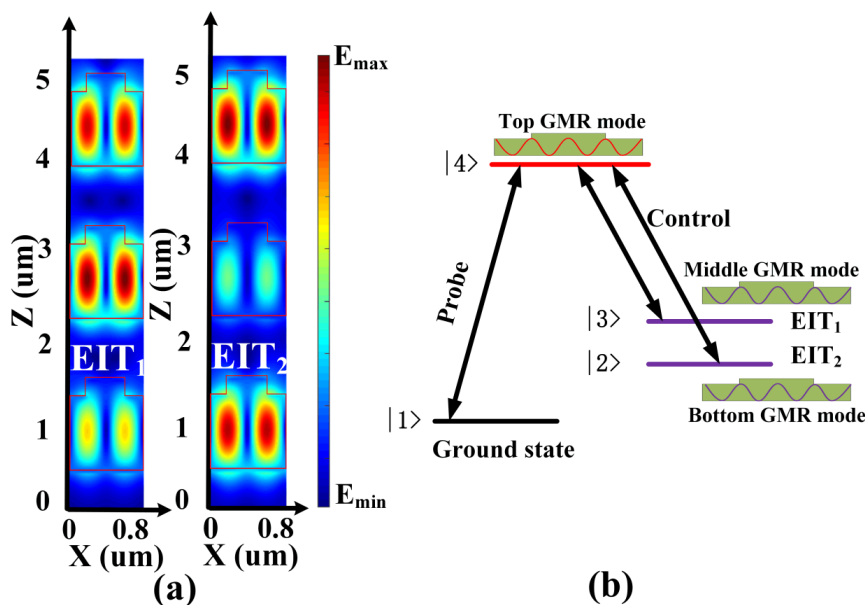


Figure 2. (a) Electric field distribution of two electromagnetically induced transparency (EIT) effects in the GMR system; (b) The analogy between the GMR system with a double EIT-like effect and a quasi- Λ four-level atomic system model.

Here, φ represents the phase accumulation from grating G₁ to grating G₂ (G₃), n_{eff} represents the effective refractive index from grating G₁ to grating G₂ (G₃), S represents the optical distance from grating G₁ to grating G₂ (G₃), and λ is the response wavelength of EIT, $m \in \mathbb{N}$.

In other words, the modes in different GWLs are coupled once the optical system introduces F–P resonance. Thus, the GMR system shows two transparent peaks at 1549.95 nm and 1550.75 nm in the transmission spectrum.

The quasi- Λ four-level atomic energy system model is depicted in Figure 2b. The analogy between the GMR system and the atomic EIT system can make it easier to comprehend the physics of the double EIT-like effect. With $|1\rangle$ being the ground state in the model, the fields of the bottom GMR mode and middle GMR mode correspond to the probability amplitude of the atom at the metastable state $|2\rangle$ and $|3\rangle$, while the field of the top GMR mode is equivalent to the probability amplitude of the atom at the excited state $|4\rangle$. In addition, the probe field is the input of the top GMR mode, and the control fields are the coupling of the top GMR mode and the other two GMR modes. We observed that two EIT-like peaks appeared at the position of the probe mode after the control field was introduced [31,32]. EIT₁ corresponds to the destructive interference between direct transition pathway $|1\rangle \rightarrow |4\rangle$ and indirect transition pathway $|1\rangle \rightarrow |4\rangle \rightarrow |3\rangle \rightarrow |4\rangle$, and EIT₂ corresponds to the interference between transition pathways $|1\rangle \rightarrow |4\rangle$ and $|1\rangle \rightarrow |4\rangle \rightarrow |2\rangle \rightarrow |4\rangle$.

A narrow transparent window is usually associated with steep dispersion, which leads to a lower group velocity of light propagation; that is, slow light is a typical feature of the EIT effect. The spectral distribution of two EITs shows that there is extreme dispersion change near the two transparent windows. In the normal dispersion zone, the group velocity can be slower than c (the speed of light in vacuum), and slow light can be obtained [33]. There will also be fast light in the anomalous dispersion area, but we only pay attention to the slow light effect here. The performance of slow light can be determined by the optical delay time τ and the group index n_g , which are defined as follows [34]:

$$\tau = \frac{d\varphi(\omega)}{d\omega} \quad (2)$$

$$n_g = \frac{c}{v_g} = \frac{c}{L} \tau \quad (3)$$

In Equations (2) and (3), $\varphi(\omega)$ represents the transmission phase shift from the incident light to the phase monitor (placed at the bottom of GWL₃), c is the speed of light, n_g is the group velocity in the GMR system, and L is the length of the GMR system (from the top of the SiO₂ coating to the bottom of GWL₃). Using optical delay time to evaluate slow light performance is more precise as a result of different devices having different lengths. Figure 3a,b illustrate the phase shift and optical delay time of the double EIT-like effect shown in Figure 1. The two oblique phase shifts correspond to the two transparent windows. A positive delay time represents slow light, while a negative one is fast light. Two delay times of 22.59 ps and 8.43 ps are respectively generated near the two EIT peaks. Compared with other research using grating and the GMR effect to achieve slow light [35–37], our work had a quite excellent optical delay time, as shown in Table 1. Moreover, we obtained dual-channel slow light.

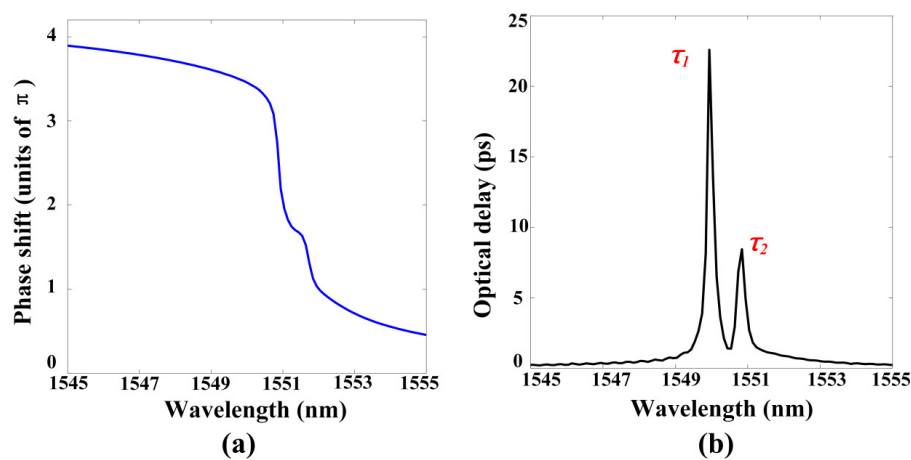


Figure 3. (a) The spectrum of phase shift in the GMR system with the double EIT-like effect in Figure 1; (b) The spectrum of delay time in the GMR system with the double EIT-like effect in Figure 1.

Table 1. Delay time compared to other slow light works based on grating and the GMR effect.

Reference	τ_1 (ps)	τ_2 (ps)
this work	22.59	8.43
35	29.73	–
36	21.80	–
37	3.10	–

4. Discussion

Our previous research using the GMR effect to achieve the EIT-like effect in WGS [20,21] has discussed extensively and in depth the influence of parameters such as the width and period of the grating and the spacing between two GWLs on the transparent window. At the same time, while the

response wavelengths of the GMR modes in different GWLs in the previous works were the same, the effect of the wavelength detuning between two different GMR modes on the transparent window has not been discussed. Here, we adjusted the wavelength detuning of the two GMR modes by changing the width of the grating to investigate the double EIT-like effect.

The transmission spectra and delay time at different W_2 (different δ_1) are given in Figure 4. We define the wavelength detuning of the top GMR mode and the middle GMR mode as δ_1 , where $\delta_1 = \lambda_{GMR1} - \lambda_{GMR2}$. In Figure 4a–d, W_2 decreases from 380 nm to 335 nm, the detuning amount δ_1 increases from 0.93 nm to 3.25 nm (λ_{GMR1} remains unchanged, λ_{GMR2} gradually decreases, and λ_{GMR3} is the same as λ_{GMR1} but not shown in Figure 4), EIT₁ is blue-shifted from 1549.34 nm to 1547.45 nm, while the position of EIT₂ remains unchanged. In order to show this more clearly, we present in Figure 4e the resonance wavelengths λ_1 and λ_2 of the two transparent windows under different W_2 (different δ_1). To study the effect of the detuning amount δ_1 on the slow light performance, the corresponding delay time spectrum is given in Figure 4f. The delay time τ_2 is kept around 10 ps, but the delay time τ_1 decreases from 16.94 ps to 5.03 ps, since as the detuning δ_1 increases, the coupling between the top GMR mode and the middle GMR mode becomes weaker.

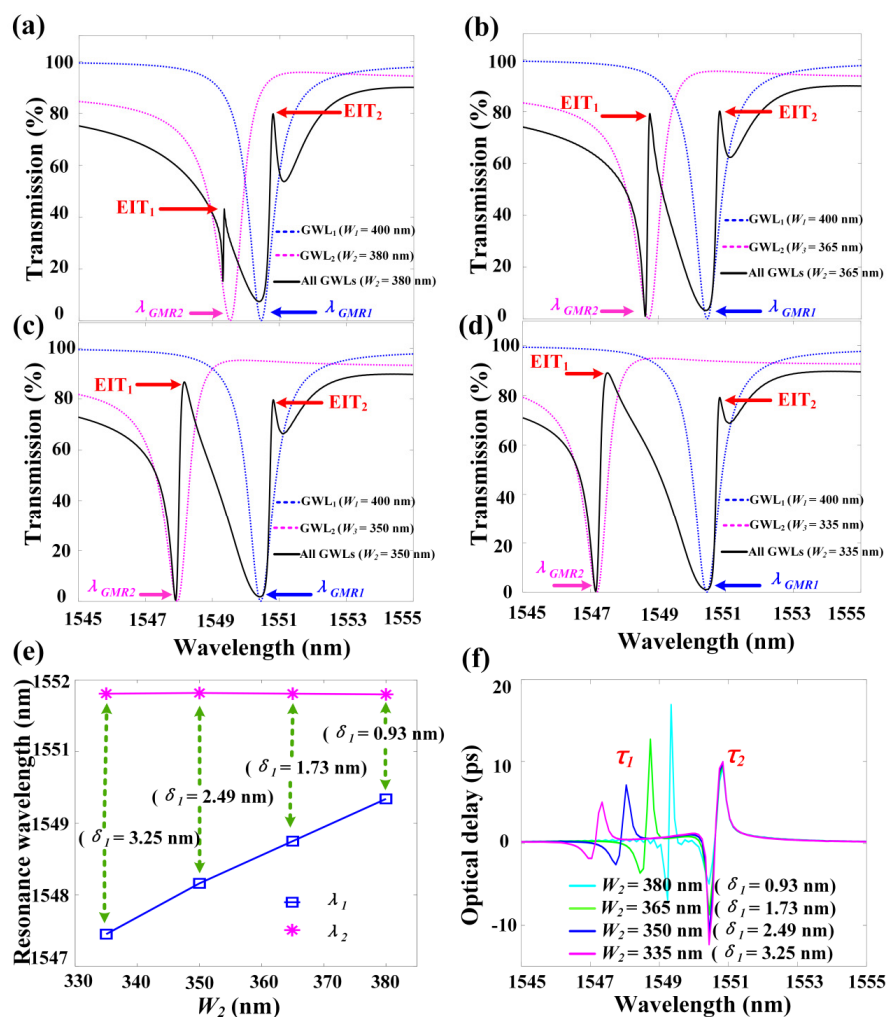


Figure 4. The transmission spectra and delay time under different W_2 (different δ_1); other parameters are the same as in Figure 1. (a) The transmission spectrum of the system when $W_2 = 380$ nm ($\delta_1 = 0.93$ nm); (b) The transmission spectrum of the system when $W_2 = 365$ nm ($\delta_1 = 1.73$ nm); (c) The transmission spectrum of the system when $W_2 = 350$ nm ($\delta_1 = 2.49$ nm); (d) The transmission spectrum of the system when $W_2 = 335$ nm ($\delta_1 = 3.25$ nm); (e) Two resonant wavelengths of two EITs under different W_2 (different δ_1); (f) Two delay times under different W_2 (different δ_1).

Figure 5 demonstrates the transmission spectra and delay time under different W_3 (different δ_2). We define the wavelength detuning of the top GMR mode and the bottom GMR mode as δ_2 , where $\delta_2 = \lambda_{GMR3} - \lambda_{GMR1}$. It can be clearly seen that W_3 increases from 415 nm (in Figure 5a) to 460 nm (in Figure 5d), and δ_2 increases from 0.35 nm to 2.88 nm (λ_{GMR1} remains unchanged, λ_{GMR3} gradually increases, and λ_{GMR2} is equal to λ_{GMR1} but not shown in Figure 5). The position of EIT₁ remains basically unchanged, while EIT₂ is red-shifted from 1550.91 nm to 1551.97 nm. The resonance wavelengths of the two EITs at different W_3 (different δ_2) in Figure 5e show this more clearly. In order to explore the relationship between the detuning amount δ_2 and the slow light performance, the delay time spectrum under different W_3 (different δ_2) is depicted in Figure 5f. Obviously, the delay time τ_1 remains at ~30 ps, while as W_3 increases, δ_2 gradually increases. The delay time τ_2 decreases significantly because the coupling between the top GMR mode and the bottom GMR mode becomes weaker.

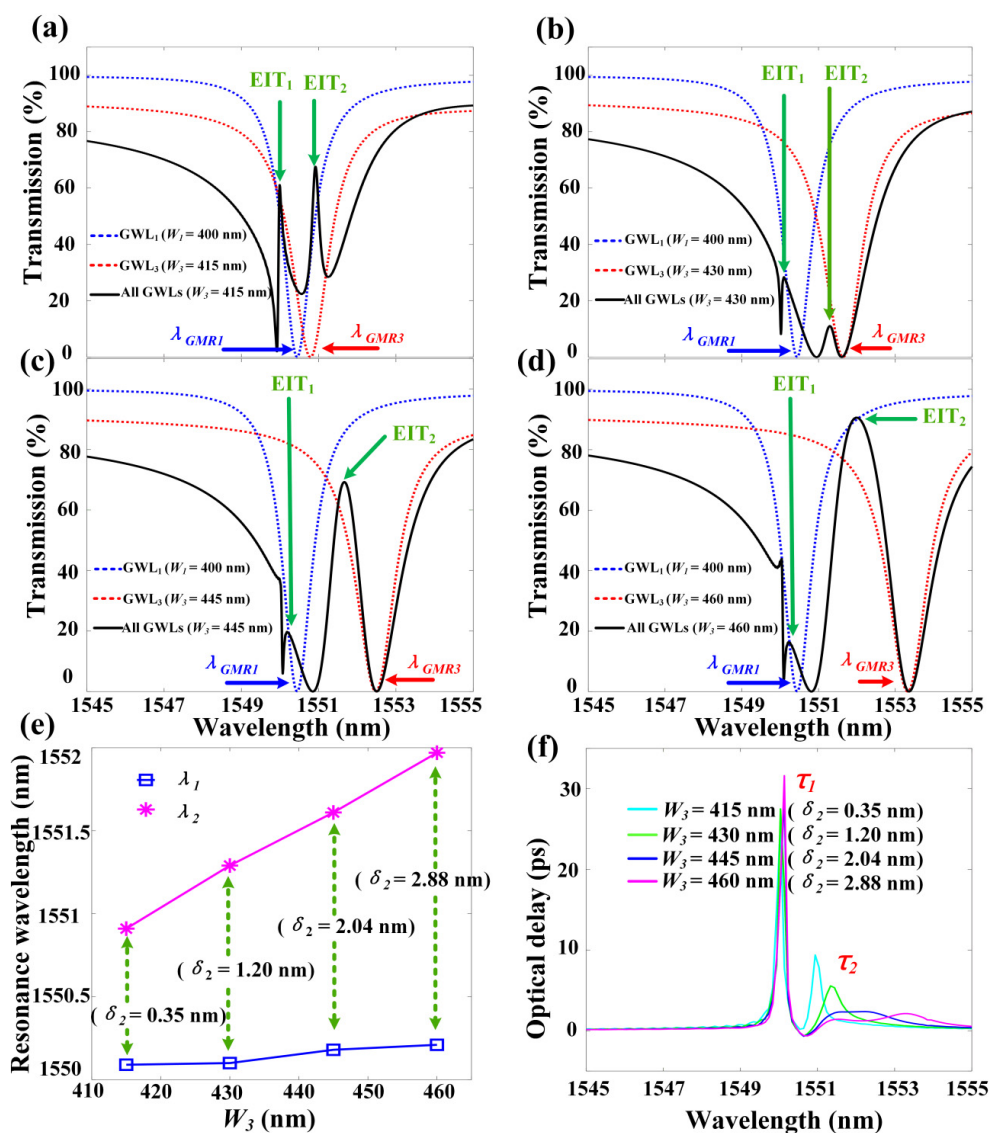


Figure 5. The transmission spectra and delay time under different W_3 (different δ_2); other parameters are the same as in Figure 1. (a) The transmission spectrum of the system when $W_3 = 415$ nm ($\delta_2 = 0.35$ nm); (b) The transmission spectrum of the system when $W_3 = 430$ nm ($\delta_2 = 1.20$ nm); (c) The transmission spectrum of the system when $W_3 = 445$ nm ($\delta_2 = 2.04$ nm); (d) The transmission spectrum of the system when $W_3 = 460$ nm ($\delta_2 = 2.88$ nm); (e) Two resonant wavelengths of two EITs under different W_3 (different δ_2); (f) Two delay times under different W_3 (different δ_2).

The previous parameter discussion showed that the response wavelength detuning of different GMR modes will affect the position of the transparent window. We reduced the width W_3 of the grating G_3 to make the EIT_2 blue shift close to EIT_1 , so that we obtained a wide-band flat-top transparent window (as shown in Figure 6a). The wide-band flat-top transparent window had a top bandpass width of about 0.72 nm and a peak transmittance of about 57%. The corresponding delay time spectrum is illustrated in Figure 6b. It can be seen that the delay time at the position of the transparent window is all above 2.4 ps. This not only provides an idea for the design of slow optical devices with a wide-band flat-top window but also can be used as a wide-band filter, where flat-top features can be used to separate each communication channel in optical communications applications.

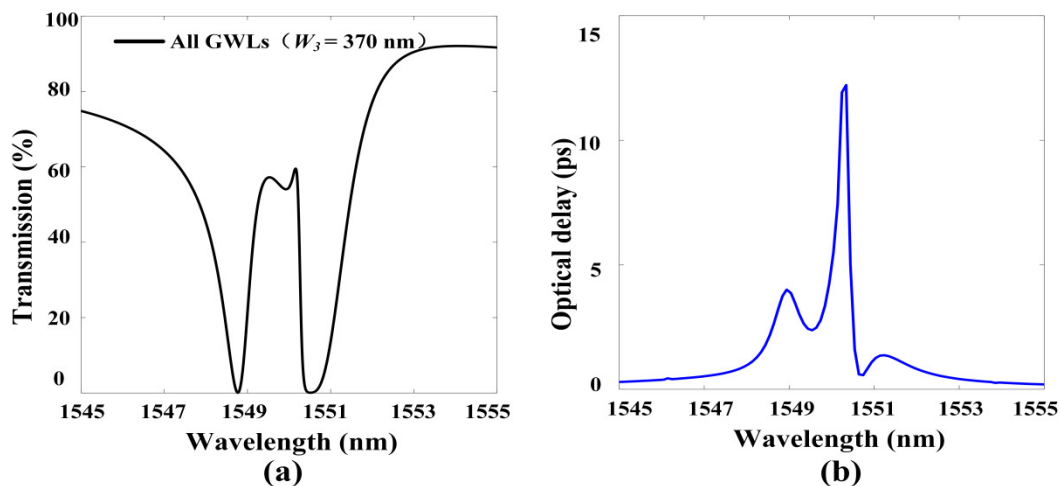


Figure 6. (a) Transmission spectrum of a wide-band flat-top transparent window, where the structural parameters are $W_1 = W_2 = 400$ nm, $W_3 = 370$ nm; other parameters are the same as those in Figure 1; (b) The delay time spectrum corresponding to the wide-band flat-top transparent window.

5. Conclusions

In conclusion, we investigated the double EIT-like effect in the GMR system with three resonance grating cascade structures. This work provides a way to accomplish the double EIT-like effect by utilizing the GMR effect. The different GMR modes in the GWLs begin to couple once an F–P resonator is introduced, and two narrow-band transparent windows appear simultaneously in a transmission dip. We not only obtained quite excellent dual-channel slow light but also examined the effect of the wavelength detuning between different GMR modes on the position of the transparent window by changing the grating width. Meanwhile, a wide-band flat-top transparent window was also achieved by appropriately adjusting the wavelength detuning between different GMR modes. This work provides a method to achieve the double EIT-like effect, which not only has potential applications in dual-channel slow light devices but also in the field of optical communications.

Author Contributions: Conceptualization, G.L. and Y.H.; methodology, G.L. and Y.H.; software, Z.Z. (Zhaojian Zhang), Y.T., L.Z. and H.H.; validation, G.L. and Y.H.; formal analysis, G.L., J.Y., and Y.H.; investigation, Y.H.; resources, J.Y. and Z.Z. (Zhenrong Zhang); data curation, G.L.; writing—original draft preparation, G.L.; writing—review and editing, Y.H., J.Y., Z.Z. (Zhenrong Zhang), and Z.Z. (Zhaojian Zhang); visualization, G.L.; supervision, Y.H., J.Y., and Z.Z. (Zhenrong Zhang); project administration, Y.H., J.Y., and Z.Z. (Zhenrong Zhang); funding acquisition, J.Y. and Z.Z. (Zhenrong Zhang). All authors have read and agreed to the published version of the manuscript.

Funding: This work was supported by the National Natural Science Foundation of China (60907003, 61805278), the China Postdoctoral Science Foundation (2018M633704), the Foundation of NUDT (JC13-02-13, ZK17-03-01), the Hunan Provincial Natural Science Foundation of China (13JJ3001, 2020JJ5646), the Program for New Century Excellent Talents in University (NCET-12-0142), the National Natural Science Foundation of China (61661004), and Guangxi Science Foundation (2017GXNSFAA198227).

Conflicts of Interest: The authors declare no conflict of interest.

References

1. Kocharovskaya, A.; Khanin, Y.I. Population trapping and coherent bleaching of a three-level medium by a periodic train of ultrashort pulses. *Zh. Eksp. Teor. Fiz* **1986**, *90*, 1610–1618.
2. Harris, S.E.; Yin, G.Y.; Kasapi, A.; Jain, M.; Luo, Z.F. Electromagnetically induced transparency. In *Coherence and Quantum Optics VII*; Springer: Boston, MA, USA, 1997; pp. 295–304. [[CrossRef](#)]
3. Strelniker, Y.M.; Bergman, D. Transmittance and transparency of subwavelength-perforated conducting films in the presence of a magnetic field. *Phys. Rev. B* **2008**, *77*, 205113. [[CrossRef](#)]
4. Hau, L.V.; Harris, S.E.; Dutton, Z.; Behroozi, C.H. Light speed reduction to 17 metres per second in an ultracold atomic gas. *Nature* **1999**, *397*, 594–598. [[CrossRef](#)]
5. Khurgin, J.B.; Tucker, R.S. *Slow Light: Science and Applications*, 1st ed.; CRC Press: Boca Raton, FL, USA, 2008.
6. Huang, Y.; Min, C.; Veronis, G. Subwavelength slow-light waveguides based on a plasmonic analogue of electromagnetically induced transparency. *Appl. Phys. Lett.* **2011**, *99*, 143117. [[CrossRef](#)]
7. Wei, Z.; Li, X.; Zhong, N.; Tan, X.; Zhang, X.; Liu, H.; Meng, H.; Liang, R. Analogue Electromagnetically Induced Transparency Based on Low-loss Metamaterial and its Application in Nanosensor and Slow-light Device. *Plasmonics* **2017**, *12*, 641–647. [[CrossRef](#)]
8. Ilchenko, V.S.; Savchenkov, A.A.; Matsko, A.B.; Maleki, L. Nonlinear optics and crystalline whispering gallery mode cavities. *Phys. Rev. Lett.* **2004**, *92*, 043903. [[CrossRef](#)]
9. Xiao, Y.F.; Özdemir, Ş.K.; Gaddam, V.; Dong, C.H.; Imoto, N.; Yang, L. Quantum nondemolition measurement of photon number via optical Kerr effect in an ultra-high-Q microtoroid cavity. *Opt. Express* **2008**, *16*, 21462–21475. [[CrossRef](#)]
10. Fan, S. Sharp asymmetric line shapes in side-coupled waveguide-cavity systems. *Appl. Phys. Lett.* **2002**, *80*, 908–910. [[CrossRef](#)]
11. Chao, C.Y.; Guo, L.J. Biochemical sensors based on polymer microrings with sharp asymmetrical resonance. *Appl. Phys. Lett.* **2003**, *83*, 1527–1529. [[CrossRef](#)]
12. Xiao, Y.F.; He, L.; Zhu, J.; Yang, L. Electromagnetically induced transparency-like effect in a single polydimethylsiloxane-coated silica microtoroid. *Appl. Phys. Lett.* **2009**, *94*, 231115. [[CrossRef](#)]
13. Shvets, G.; Wurtele, J.S. Transparency of magnetized plasma at the cyclotron frequency. *Phys. Rev. Lett.* **2002**, *89*, 115003. [[CrossRef](#)] [[PubMed](#)]
14. Liu, N.; Langguth, L.; Weiss, T.; Kästel, J.; Fleischhauer, M.; Pfau, T.; Giessen, H. Plasmonic analogue of electromagnetically induced transparency at the Drude damping limit. *Nature Mater.* **2009**, *8*, 758–762. [[CrossRef](#)] [[PubMed](#)]
15. Singh, R.; Rockstuhl, C.; Lederer, F.; Zhang, W. Coupling between a dark and a bright eigenmode in a terahertz metamaterial. *Phys. Rev. B* **2009**, *79*, 085111. [[CrossRef](#)]
16. Zhang, J.; Xiao, S.; Jeppesen, C.; Kristensen, A.; Mortensen, N.A. Electromagnetically induced transparency in metamaterials at near-infrared frequency. *Opt. Express* **2010**, *18*, 17187–17192. [[CrossRef](#)]
17. Lee, S.G.; Jung, S.Y.; Kim, H.S.; Lee, S.; Park, J.M. Electromagnetically induced transparency based on guided-mode resonances. *Opt. Lett.* **2015**, *40*, 4241–4244. [[CrossRef](#)] [[PubMed](#)]
18. Lee, S.G.; Kim, S.H.; Kim, K.J.; Kee, C.S. Polarization-independent electromagnetically induced transparency-like transmission in coupled guided-mode resonance structures. *Appl. Phys. Lett.* **2017**, *110*, 111106. [[CrossRef](#)]
19. Sun, Y.; Chen, H.; Li, X.; Hong, Z. Electromagnetically induced transparency in planar metamaterials based on guided mode resonance. *Opt. Commun.* **2017**, *392*, 142–146. [[CrossRef](#)]
20. Han, Y.; Yang, J.; He, X.; Huang, J.; Zhang, J.; Chen, D.; Zhang, Z. High quality factor electromagnetically induced transparency-like effect in coupled guided-mode resonant systems. *Opt. Express* **2019**, *27*, 7712–7718. [[CrossRef](#)]
21. Li, G.; Yang, J.; Zhang, Z.; Wen, K.; Tao, Y.; Han, Y.; Zhang, Z. Double Spectral Electromagnetically Induced Transparency Based on Double-Bar Dielectric Grating and Its Sensor Application. *Appl. Sci.* **2020**, *10*, 3033. [[CrossRef](#)]
22. Ko, Y.H.; Magnusson, R. Flat-top bandpass filters enabled by cascaded resonant gratings. *Opt. Lett.* **2016**, *41*, 4704–4707. [[CrossRef](#)]

23. Yamada, K.; Lee, K.J.; Ko, Y.H.; Inoue, J.; Kintaka, K.; Ura, H.; Magnusson, R. Flat-top narrowband filters enabled by guided-mode resonance in two-level waveguides. *Opt. Lett.* **2017**, *42*, 4127–4130. [[CrossRef](#)] [[PubMed](#)]
24. Doskolovich, L.L.; Bezus, E.A.; Bykov, D.A. Integrated flat-top reflection filters operating near bound states in the continuum. *Photon. Res.* **2019**, *7*, 1314–1322. [[CrossRef](#)]
25. Doskolovich, L.L.; Bezus, E.A.; Bykov, D.A.; Golovastikov, N.V.; Soifer, V.A. Resonant properties of composite structures consisting of several resonant diffraction gratings. *Opt. Express* **2019**, *27*, 25814–25828. [[CrossRef](#)] [[PubMed](#)]
26. Chen, J.; Chu, P. Phase-induced Fano antiresonance in a planar waveguide with two dielectric ridges. *J. Opt. Soc. Am. B* **2019**, *36*, 3417–3427. [[CrossRef](#)]
27. Malitson, I.H. Interspecimen comparison of the refractive index of fused silica. *J. Opt. Soc. Am.* **1965**, *55*, 1205–1209. [[CrossRef](#)]
28. Kischkat, J.; Peters, S.; Gruska, B.; Semtsiv, M.; Chashnikova, M.; Klinkmüller, M.; Fedosenko, O.; Machulik, S.; Aleksandrova, A.; Monastyrskyi, G.; et al. Mid-infrared optical properties of thin films of aluminum oxide, titanium dioxide, silicon dioxide, aluminum nitride, and silicon nitride. *Appl. Opt.* **2012**, *51*, 6789–6798. [[CrossRef](#)]
29. Papanikolaou, N.; Fedotov, V.A.; Zheludev, N.I.; Prosvirnin, S.L. Metamaterial analog of electromagnetically induced transparency. *Phys. Rev. Lett.* **2008**, *101*, 253903. [[CrossRef](#)]
30. Kekatpure, R.D.; Barnard, E.S.; Cai, W.; Brongersma, M.L. Phase-coupled plasmon-induced transparency. *Phys. Rev. Lett.* **2010**, *104*, 243902. [[CrossRef](#)]
31. Fleischhauer, M.; Imamoglu, A.; Marangos, J.P. Electromagnetically induced transparency: Optics in coherent media. *Rev. Mod. Phys.* **2005**, *77*, 633. [[CrossRef](#)]
32. Liu, Y.C.; Li, B.B.; Xiao, Y.F. Electromagnetically induced transparency in optical microcavities. *Nanophotonics* **2017**, *6*, 789–811. [[CrossRef](#)]
33. Bigelow, M.S.; Lepeshkin, N.N.; Boyd, R.W. Superluminal and slow light propagation in a room-temperature solid. *Science* **2003**, *301*, 200–202. [[CrossRef](#)] [[PubMed](#)]
34. Zhang, Z.; Yang, J.; He, X.; Han, Y.; Zhang, J.; Huang, J.; Chen, D.; Xu, S. Active enhancement of slow light based on plasmon-induced transparency with gain materials. *Materials* **2018**, *11*, 941. [[CrossRef](#)] [[PubMed](#)]
35. Magnusson, R.; Shokooh-Saremi, M.; Wang, X. Dispersion engineering with leaky-mode resonant photonic lattices. *Opt. Express* **2010**, *18*, 108–116. [[CrossRef](#)]
36. Chen, Y.; Zhang, Z.; Yu, M. Tunable out-of-plane slow light in resonance induced transparent grating waveguide structures. *Appl. Phys. Lett.* **2013**, *103*, 061109. [[CrossRef](#)]
37. Tang, B.; Dai, L.; Jiang, C. Transmission enhancement of slow light by a subwavelength plasmon-dielectric system. *J. Opt. Soc. Am. B* **2010**, *27*, 2433–2437. [[CrossRef](#)]

